Fretting fatigue crack propagation rate under variable loading conditions

C. Gandiolle, S. Fouvry
LTDS, Ecole Centrale de Lyon, 36 avenue Guy de Collonges, 69134 Ecully Cedex, France
camille.gandiolle@ec-lyon.fr, siegfried.fouvry@ec-lyon.fr

ABSTRACT. Fretting fatigue experiments aim to represent industrial problems and most of them endure variable loading. Being able to assess lifetime of assemblies, especially for low propagation rate conditions, is essential as experimental validation is often too expensive. Both experimental and numerical approaches are proposed to follow the crack propagation rate of steel on steel cylinder/plane fretting fatigue contact submitted to variable loading conditions.
An original experimental monitoring has been implemented on the fretting-fatigue test device to observe crack propagation using a potential drop technique. A calibration curve relating crack length and electrical potential was established for the studied contact. It allows direct knowledge of the crack length and crack propagation rate. It was applied to mixed load test showing crack arrest for the last loading condition.
To explain this behavior, a 2-dimensional FE modeling was implemented to simulate the complexes multi-axial contact stressing. The crack propagation rate was formalized using an effective stress intensity factor amplitude ΔK_{eff} coupled with Paris law of the material. The crack arrest condition for a given loading was related to ΔK_{eff} along the expected crack path crossing the material crack arrest threshold ΔK_0. The failure was related to ΔK_{eff} reaching the critical stress intensity factor K_{IC}. A good correlation with experiments was observed allowing to predict the crack arrest condition although the model tends to overestimate the final crack length extension.

KEYWORDS. Fretting fatigue; FEM; Cracking; Variable loading.

INTRODUCTION

Fretting is defined as a small oscillatory movement between two bodies in contact which induce relative displacement between the two surfaces. Combined with cyclic bulk fatigue loading, the so called fretting-fatigue loading can induce catastrophic damages such as wear or cracking, which critically reduce the endurance of assemblies. In addition, fretting fatigue experiments aim to represent industrial problems and most of them endure variable loadings.
Being able to assess lifetime of assemblies, especially for variable loading applied for very high number of cycles, is essential as experimental validation is often too expensive. This study concentrates on cracking damage and is restricted to the partial slip domain.
Crack nucleation risk is usually investigated by applying multi-axial fatigue criterion. Predictions were improved by considering the severe stress gradients imposed by the contact loading, using non-local process volume stress averaging strategy [1] or equivalent critical distance [2].

Once a crack is nucleated, depending on the loading amplitude, it will propagate or reach a crack arrest condition.
The prediction of crack arrest was addressed by Araujo et al. [3] applying a short crack regime strategy. Crack propagation and crack propagation rate are usually addressed using Paris law. Numerous models exist to predict the lifetime of assemblies. Some consider that total lifetime can be approximated by the crack nucleation life and that crack propagation is negligible [4]. Others consider only the crack propagation phase [5]. Some authors also estimate the total lifetime as the sum of the crack nucleation life and the crack propagation life [6]. In the frame of this research work we investigated how to predict the crack propagation rate and the crack arrest condition of fretting fatigue test subjected to variable loading conditions.

EXPERIMENTS

Materials

The studied material is a 32C1 steel (E=200GPa, ν=0.3). It shows low yield stress and is thus described by an elastic-plastic law. Because this study was conducted for industrial purposes, the industrial monotonic material law with isotropic hardening was used to describe the hardening of the material. Fig. 1 plots the monotonic hardening of the studied steel which was obtained from a simple tensile test and normalized by the yield strength $\sigma_{y,flat}$.
The material was tested under various fretting fatigue conditions, using a cylinder/plane contact configuration, with a cylinder of R=4.6 mm radius applied with a normal force P on the flat material. The cylinder was a FM35 steel (E=200GPa, v=0.3), but with higher yield stress ($\sigma_{y\_cylinder} >> \sigma_{y,flat}$), to investigate cracking on the plane specimen only. A similar monotonic elastic-plastic law with isotropic hardening was considered to describe its behavior (Fig. 1).

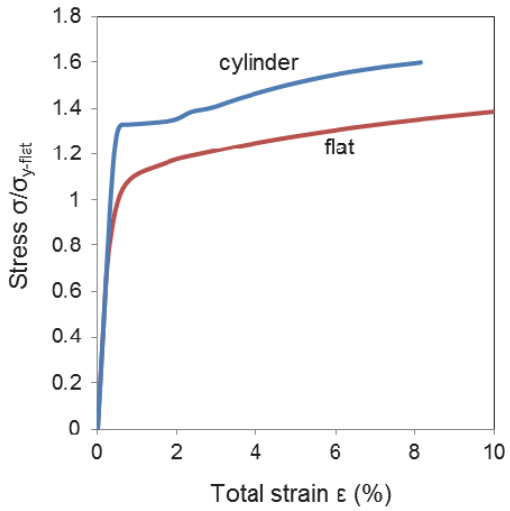

Figure 1: Monotonic elastic-plastic material laws of the flat and cylinder components (R=4.6mm).

Conventional 4 points bending tests were used to identify the crack propagation law of the study material. It follows Paris law:

$$\frac{db}{dN} = C.(\Delta K)^m \tag{1}$$

With b, the crack length and N the number of cycles. The parameter C and m were really close to the British Standard (BS) parameters disclosed in Tab. 1. The crack arrest condition was obtained for $\Delta K_{th\_10\text{-}7}=\Delta K_0=5.7$ MPa.m$^{1/2}$, and $K_{IC}=212$ MPa.m$^{1/2}$.
As several high stress ratios were applied, an effective stress intensity factor range ΔK_{eff} was preferred to describe the overall crack propagation behavior. ΔK_{eff} was established considering a simplification of Elber approximation proposed by V. Gros [7]:

For $R_K>0$; $\Delta K_{eff} = K_{1max}$-4 with $R_K = K_{Imin}/K_{Imax}$ (2)

For $-1<R_K<0$; $\Delta K_{eff} = K_{1max}-(4.R_K +4)$ (3)

For $R_K<-1$; $\Delta K_{eff} = K_{1max}$ (4)

The overall C and m parameters of the Paris law expressed as a function of ΔK_{eff} are given in Tab. 1.

$R_\sigma=\sigma_{min}/\sigma_{max}$	C	m
0.1	$8.32x10^{-9}$	2.88
0.5	$1.22x10^{-8}$	2.88
overall	$1.27x10^{-9}$	3.27

Table 1: Crack propagation laws from british standard BS7910-05

Fretting fatigue test

The fretting fatigue test device is shown in Fig. 2a. It consists in three hydraulic actuators to control independently the normal force P, the tangential force amplitude Q* and the fatigue stress σ.

The fretting actuator imposes a purely alternating sinusoidal cyclic displacement δ(t) on the plane, generating an alternating cyclic tangential load Q(t) on the contact surface. During the test, displacement δ, normal force P and tangential force Q were recorded, enabling the Q-δ fretting loop to be plotted and thus the fretting regime to be identified. As cracking, and more specifically crack nucleation, was to be investigated, the displacements were kept small enough to maintain partial slip conditions.

Sinusoidal cyclic tangential force and fatigue forces were applied in phase. That is the maximum fretting load Q^*_{max} was applied at the same time as the maximum fatigue stress σ_{max}. All tests were performed at constant normal force P. The frequency was fixed at 12 Hertz, high enough to investigate a long test condition and low enough to guarantee test control stability. The fretting stress ratio was kept constant at $R_{Q^*} = Q^*_{min}/Q^*_{max} = -Q^*/+Q^* = -1$.

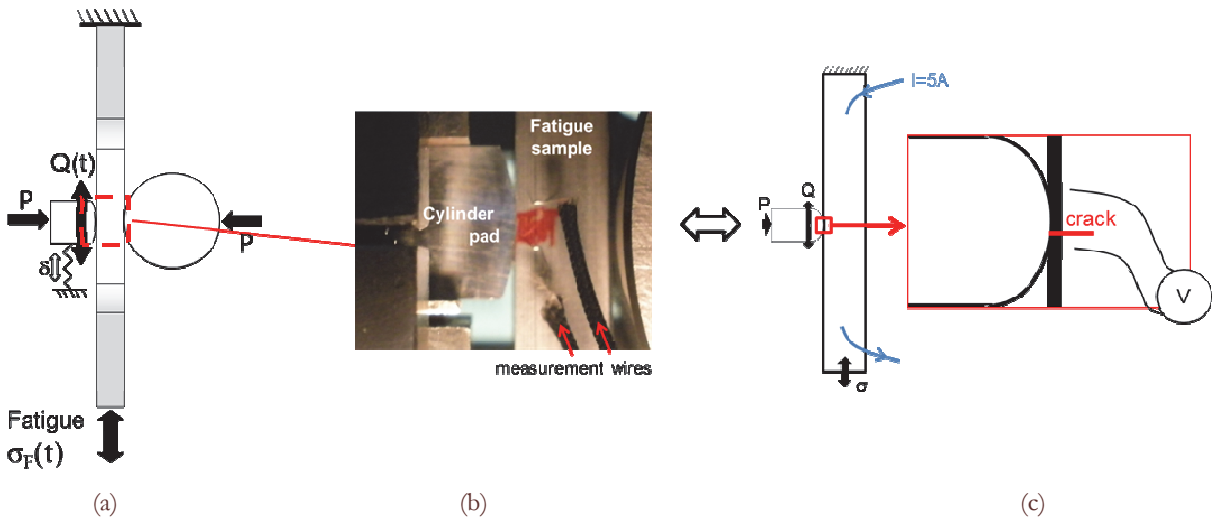

Figure 2: (a) sketch of the fretting fatigue test device, (b) Picture of the fretting fatigue contact with the measurement wires, (c) sketch of the implementation of the PDT method.

A monitoring system using the potential drop technique method was implemented on the fretting fatigue sample. The potential drop technique (PDT) allows direct information on the crack propagation kinetic during test. It was introduced in 1957 by Barnette et Troiono to observe crack propagation in fatigue tests [8], and first applied on fretting fatigue test by Kondo et al. [9]. Since then, the technique has been widely used. Fig. 2b&c show a picture and a sketch of the application of PDT on a fretting fatigue test.

A continuous current I=5A is applied through the fatigue test sample. The contact potential is measured between two platinum wires, of 0.1mm of diameter, welded on the sample surface. The potential is measured on each side of the sample in order to take into account the possible non homogeneity of the crack propagation. The potential measured depends on the sample resistance. When a crack nucleates and propagates, the sample cross section diminishes and thus the electrical resistance increases. It is then possible to establish a calibration curve linking the crack length to the measured potential.

EXPERIMENTAL RESULTS

Crack propagation calibration curve

The calibration curve of the studied contact was established following an empirical method like Meriaux et al [10]. Considering a constant fretting fatigue solicitation of: R=4.6mm, P, $\sigma_{F,moy}/\sigma_{y,flat}$ =0.78, R_σ=0.85, Q*/P=0.30 ; tests were interrupted after various number of fretting fatigue cycles. Crack lengths were measured by destructive method [11] and plotted as a function of electrical potential (Fig. 3). Potential values of each test were normalized by their respective initial value V_0.

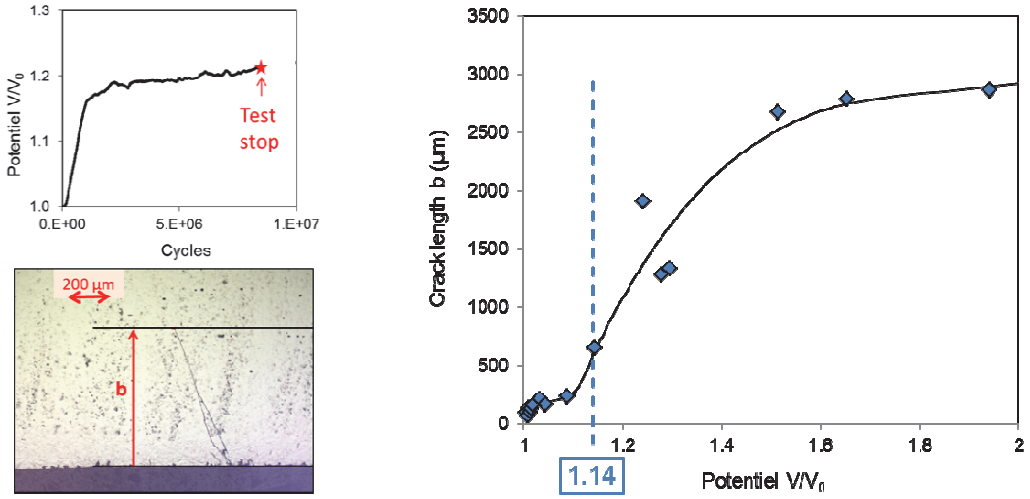

Figure 3: Identification of the calibration curve (R=4.6mm, P, $\sigma_{F,moy}/\sigma_{y,flat}$=0.78, R_F=0.85, Q*/P=0.30).

Fig. 3 plots the calibration curve. Its evolution is complex and was described by 2 successive polynomial functions:

$$\text{For } 1.01 < V/V_0 < 1.14 : b_p = 643212.(V/V_0)^3 - 2040300.(V/V_0)^2 + 2157715.(V/V_0) - 760573 \quad (5)$$

$$\text{For } 1.14 < V/V_0 : b_p = 5487.(V/V_0)^3 - 30610.(V/V_0)^2 + 57230.(V/V_0) - 33000 \quad (6)$$

We have no clear hypothesis to explain the plateau evolution observed for a crack length of b=200µm. Meriaux et al. observed a similar behavior on Ti-6AL-4V [10]. A first hypothesis suggests that it is induced by the fretting solicitation: the plateau corresponds to the change of crack propagation mode from a mixed mode I and II (fretting fatigue) to pure mode I. A second hypothesis states that the plateau could be connected to the presence of debris in the crack, in particular in the zone dominated by the mode II, which could perturb the electric conduction.
Close to the breaking points, there was a high dispersion of crack lengths which results in a second plateau.
From this curve, it can also be deduced that when the potential stabilizes then a crack arrest condition is reached. This point was studied thoroughly in a previous work [12]. A crack propagation criterion was established from the slope of the potential as a function of fretting fatigue cycles K_e.

- $K_e < 10^{-9}$cycles^{-1}: crack arrest;
- $K_e > 10^{-9}$cycles^{-1}: crack propagation.

Experimental identification of fretting fatigue crack propagation rate

The potential drop technique was applied on the following solicitation: P, $\sigma_{F,moy}/\sigma_{y,flat}$=0.78, R_F=0.85, Q*/P=0.30. Fig. 4 plots the obtained potential and the crack propagation calculated from the calibration curve. The crack nucleates around $N_{CN}=10^5$ cycles, and propagates slowly until b=300µm. then the propagation rate increases until failure at $N_T=1.73x10^6$ cycles for a final crack length of b_T=2.8 mm. The propagation life is easily deduced: $N_P=N_T-N_{CN}=1.63x10^6$ cycles.
The crack initiation time is less than 6% of the total lifetime of the contact. The crack initiation life will thus be neglected in the lifetime prediction.

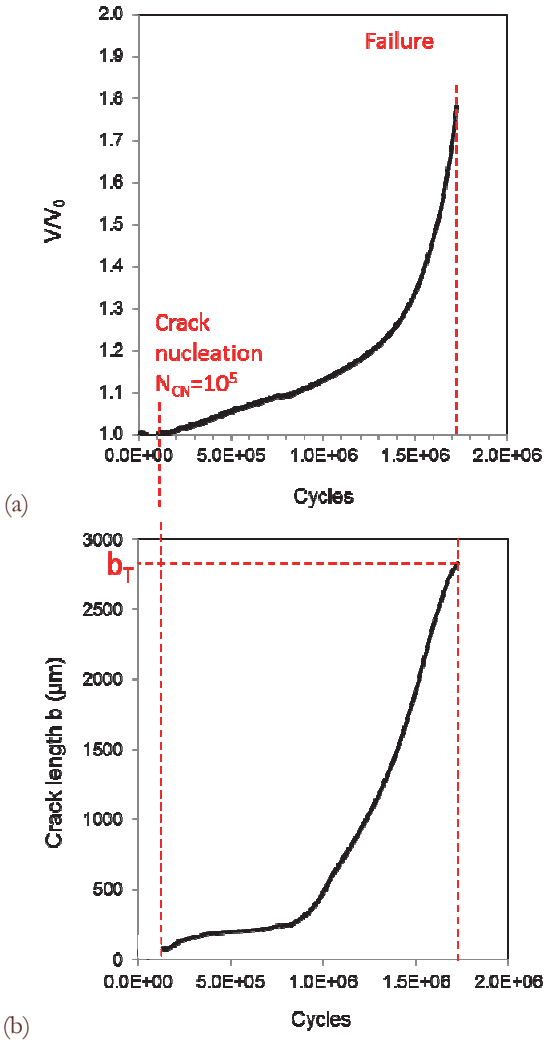

Figure 4: (a) Potential as a function of the number of cycles, (b) crack length as a function of the number of cycles calculated with the calibration curve. (R=4.6mm, P, $\sigma_{F,moy}/\sigma_{y,flat}$=0.78, R_F=0.85, Q*/P=0.30).

PREDICTION OF CRACK PROPAGATION RATE

Finite Element analysis

Finite element (FE) analysis was carried out using Abaqus 6.10 software. A 2D plain strain model of the fretting fatigue test was generated (Fig. 5a). The dimensions and boundary conditions matched the parameters of the physical experiment. The model was meshed with CPE3-type linear triangular elements, except in the contact zone where CPE4R-type linear quadrilateral elements were used; this zone was also meshed more densely than the other regions (5µm squares).

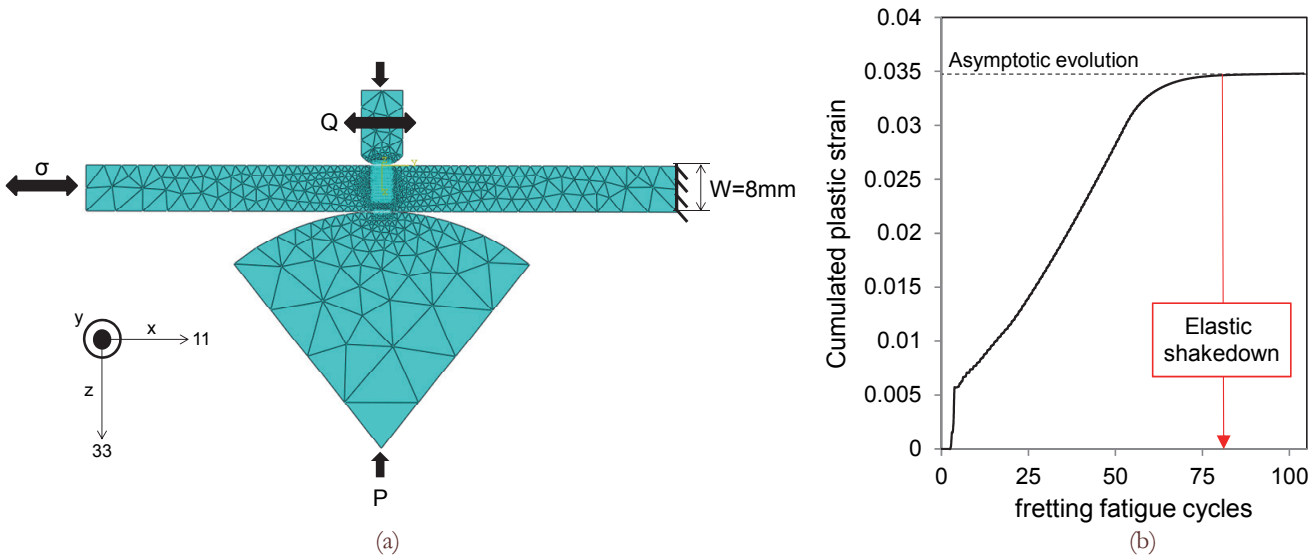

Figure 5: (a) Abaqus model of the test. (b) Cumulative plastic strain evolution simulated at the contact border hot spot for a crack arrest condition using the monotonic elastic-plastic law for the study material (P, $\sigma_{F,moy}/\sigma_{y,flat}$=0.78, R_F=0.85, Q*/P=0.30).

Surface-to-surface discretization with small sliding was adopted for contact accommodation. The Lagrange multiplier was selected as the contact algorithm. The friction coefficient of the contact μ was determined experimentally using the variable displacement technique described by Voisin et al. [14], μ=1.0. The cylinder and fatigue plane sample behaviors were described by the monotonic plastic laws introduced in Fig. 1.

The normal force with which the cylinder was applied to the plane was high enough to generate plasticity. The added fatigue loading contributed to extend the plastic state. For each simulation, the most highly strained integration point was monitored and its cumulative plastic strain evolution was plotted as a function of the fretting fatigue loading cycles (Fig. 5b). The level of activated plasticity decreased after each cycle, due partly to material hardening but mostly to plastic accommodation of the contact geometry. So the cumulative plastic strain increased until reaching an asymptotic evolution, i.e. a stable state corresponding to elastic shakedown.

Numerical analysis showed that elastic shakedown was achieved after around 80 loading cycles for fretting fatigue. Fatigue analysis was therefore performed on the stable elastic shakedown state.

Crack propagation rate identification

A decoupled approach was used to predict the crack propagation. First the contact stress state was obtained by finite elements modeling (FEM), then the normal stressing along the expected crack path are extracted at the contact border for the maximum and minimum loading conditions as schematized in Fig. 6.

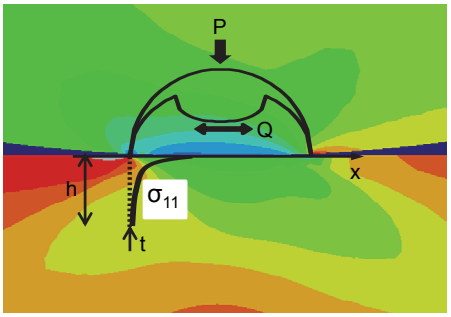

Figure 6. Stress extraction along crack path for a fretting fatigue case.

Then the mode I stress intensity factor (SIF) was calculated using Bueckner weight function approach [13]:

$$K_I = \sqrt{\frac{2}{\pi}} \int_0^h M(t).\sigma_x(t).dt \tag{7}$$

with

$$M(t) = t^{-1/2}.\left[1 - m_1.\frac{t}{h} + m_2.\left(\frac{t}{h}\right)^2\right] \tag{8}$$

and

$$m_i = A_i + B_i r^2 + C_i r^6 \tag{9}$$

with $A_1=A_{ref}$, $B_1=27.9558A_{ref}$, $C_1=14.2870A_{ref}$, $A_2=0.4070A_{ref}$, $B_2=5.3504A_{ref}$ and $C_2=113.9489A_{ref}$.
The contribution of mode II was neglected [1]. Finally the effective stress intensity range is obtained following the Eqs. 2 to 4.
Crack nucleation life was neglected following the observation of the previous paragraph. The total lifetime was thus equivalent to the propagation life. The loading cycles related to the propagation stage were computed using ΔK_{eff} integrated from b=0 up to failure:

$$N_T = N_P = \int_{b=0}^{b_T} \frac{db}{C(\Delta K)^m} \tag{10}$$

Failure was related to $K_{Imax}=K_{IC}$ with $K_{IC}=212$MPa. Alternatively, if $\Delta K_{eff}(b)$ crosses the crack arrest condition ΔK_0 then the crack stops propagating and crack arrest is reached.
Fig. 7 compares the crack length obtained from the potential drop technique with the crack length determined from the predictive method. A rather good correlation is observed. In addition the model tends to overestimate the crack extension rate which indirectly provides a conservative and safe estimation of the fretting fatigue cracking risk.

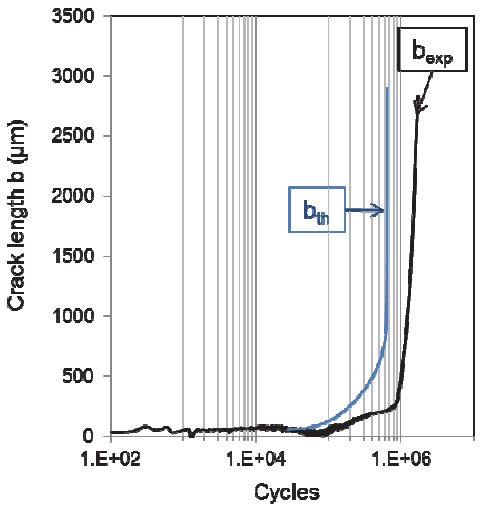

Figure 7: Comparison of experimental and theoretical crack propagation rates. (R=4.6mm, P, $\sigma_{F,moy}/\sigma_{y,flat}=0.78$, $R_F=0.85$, $Q^*/P=0.30$).

Application of prediction method to a mixed load test

Three blocks of different fretting fatigue loading were applied successively on the fretting fatigue contact (Tab. 2 and Fig. 8). Individually, block 1 led to failure (Fig. 7), block 2 led to crack arrest and block 3 generated no detectable crack.
Fig. 9a plots potential evolution of the mixed load test and Fig. 9b plots the crack propagation calculated with the calibration curve. It shows that a crack is generated at the first block and propagates throughout the first and second bloc. The crack stops propagating when the loading changes for the third block.

Bloc	$\sigma_{F,moy}/\sigma_{y\text{-}flat}$	$\sigma_{F,alt}/\sigma_{y,flat}$	Q*/P	N (cycles)
1	0.78	0.85	0.3	70000
2	0.78	1	0.3	670000
3	0.78	0.85	0.15	1000000

Table 2: Fretting fatigue loadings and durations of the mixed load test blocks

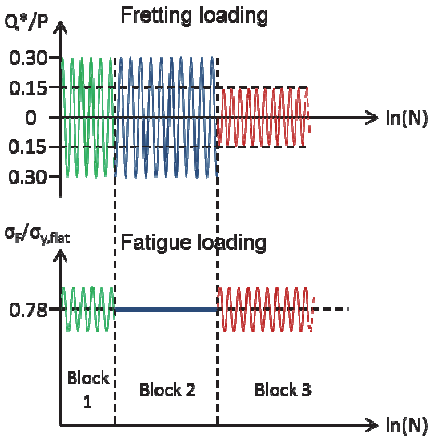

Figure 8: Sketch of loading blocks.

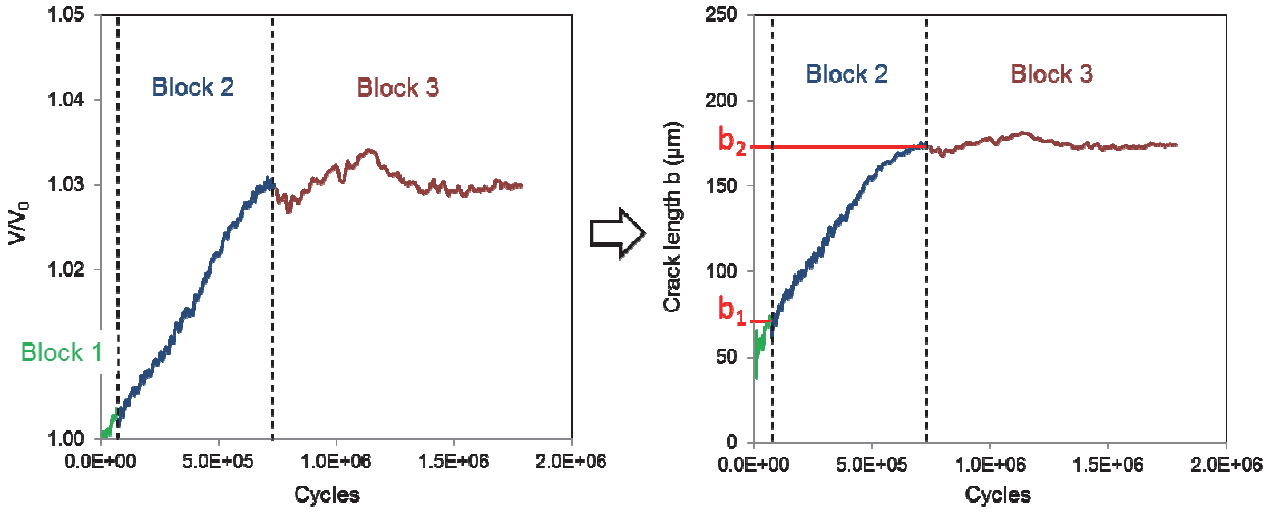

(a) (b)

Figure 9: (a) Potential evolution during mixed load test, (b) Crack propagation rate established with the calibration curve.

In order to explain this behavior, the mixed load test was simulated. Blocks were applied one after the other on the FE model as in the experimental test. Loading history, that is the residual stress from each loading block, is thus taken into account by the next block.

For each loading block, ΔK_{eff} is plotted as a function of depth in Fig. 10. Knowing crack lengths obtained at the end of each block from Fig. 9b, it is possible to shift from one curve to the other. At the end of the second bloc, crack length was equal to b_2=170µm. and at this depth, ΔK_{eff} (block 3) passes below the crack arrest threshold condition ΔK_0=5.7MPa.m$^{1/2}$. Combining these crack propagation paths evolutions, the final crack arrest condition achieved when these three loading sequences were imposed can be understood.

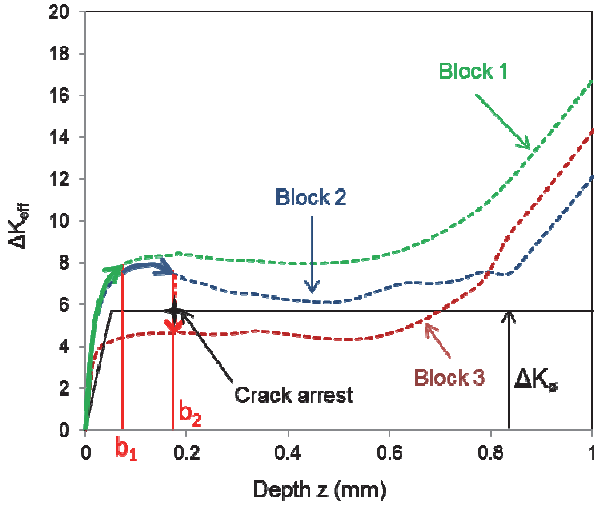

Figure 10 : Evolutions of ΔK_{eff} of each loading blocks as a function of depth.

The predictive method was applied for the studied mixed load test condition. Eq. 10 is incremented step by step and depending on N, the relevant ΔK_{eff} is considered. Fig. 11 plots the predicted crack propagation extension compared to the experimental crack propagation extension. Prediction is conservative as the predicted crack length is longer than the experimental crack length. However the predictive method recognizes the crack nucleation on the first block and the crack arrest at the third block. Hence even if the model tends to overestimate the final crack extension, it well predicts the fretting fatigue crack arrest condition.

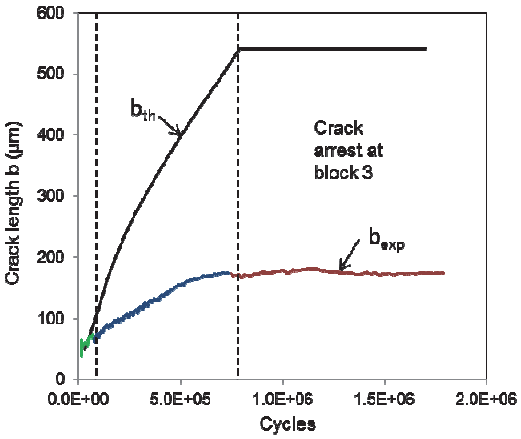

Figure 11: Comparison of theoretical crack propagation rate calculated with the predictive method and experimental crack propagation rate. Loading: R=4.6mm, P, Block 1 : $\sigma_{F,moy}/\sigma_{y,flat}$=0.78, Rσ=0.85, Q*/P=0.3, N=70000; block 2 : $\sigma_{F,moy}/\sigma_{y,flat}$=0.78, Rσ=1, Q*/P=0.3, N=670000; block 3 : $\sigma_{F,moy}/\sigma_{y,flat}$=0.78, Rσ=0.85, Q*/P=0.15, N=1000000.

Conclusion

The crack propagation rate of fretting fatigue loading was investigated both experimentally and numerically. The potential drop technique method was implemented on the fatigue fretting test device and a calibration curve was established. With this curve, the crack length was known throughout a fretting fatigue test.

A decoupled approach was applied to estimate the stress intensity factor evolution with the fretting fatigue crack extension thus to predict the crack propagation risk. The contact stress state was obtained by finite elements modeling, then the mode I stress intensity factor was calculated using a weight function approach and finally the Paris law was applied on the deduced effective stress intensity range along the crack.

It allowed for good estimation of the crack propagation rate.

Finally these strategies were applied to a mixed load test, more representative of an industrial loading case. The predictive method was adjusted to consider the successive ΔK_{eff} of each loading, depending on the number of cycles. This simple method allowed really good prediction of crack nucleation and crack arrest condition. The predicted crack extension was slightly too conservative; however it is consistent with the security coefficient needed in industry.
Better predictions may be achieved using a more representative cyclic plastic law and more elaborate description of the ΔK_{eff} parameter.

REFERENCES

[1] Fouvry, S., Kapsa, P., Vincent, L., A multiaxial fatigue analysis of fretting contact taking into account the size effect, ASTM STP., 1367 (2000) 167-182.
[2] Araújo, J., Nowell, D., The effect of rapidly varying contact stress fields on fretting fatigue, Int. J. Fatigue, 24 (2002) 763-775.
[3] Araujo, J.A., Nowell, D., Analysis of pad size effects in fretting fatigue using short crack arrest methodologies, Int. J. Fatigue, 21 (1999) 947-956.
[4] Ruiz, C., Boddington, P.H.B., Chen, K.C., An Investigation of Fatigue and Fretting in a Dovetail Joint, Exp. Mech., 24 (1984) 208-217.
[5] Giannakopoulos, A.E., Lindley, T.C., Suresh, S., Aspects of equivalence between contact mechanics and fracture mechanics: theoretical connections and a life-prediction methodology for fretting-fatigue, Acta Mater., 46 (1998) 2955-2968.
[6] Navarro, C., Munoz, S., Dominguez, J., On the use of multiaxial fatigue criteria for fretting fatigue life assessment, Int. J. Fatigue, 30 (2008) 32-44.
[7] Gros, V., Etude de l'amorçage et de la propagation des fissures de fatigue dans les essieux-axes ferroviaires, Ecole centrale Paris, 1996.
[8] Barnett, W., Troiono, A., Crack Propagation in Hydrogen Induced Brittle Fracture of Steel, J Met., 9 (1952) 94.
[9] Kondo, Y., Sakae, C., Kubota, M., Yanagihara, K., Non-propagating crack behaviour at giga-cycle fretting fatigue limit, Fatigue Fract. Eng. Mater. Struct., 28 (2005) 501-506.
[10] Meriaux, J., Fouvry, S., Kubiak, K.J., Deyber, S., Characterization of crack nucleation in TA6V under fretting-fatigue loading using the potential drop technique, Int. J. Fatigue, 32 (2010) 1658-1668.
[11] Proudhon, H., Fouvry, S., Yantio, G.R., Determination and prediction of the fretting crack initiation : introduction of the (P, Q, N) representation and definition of a variable process volume, Int. J. Fatigue, 28 (2006) 707-713.
[12] Gandiolle, C., Fouvry, S., Experimental Analysis and Modeling of the Crack Arrest Condition Under Severe Plastic Fretting Fatigue Conditions, Procedia Eng., 66 (2013) 783-792.
[13] Bueckner, H.F., Weight functions and fundamental fields for the penny shaped and the half plane crack in three spaces, Int. J. Solids Struct., 23 (1987) 57-93.
[14] Voisin, J.M., Vannes, A.B., Vincent, L., Daviot, J., Giraud, B., Analysis of a tube-grid oscillatory contact: methodology selection of superficial treatments, Wear, 181-183 (1995) 826-832.